Remote Sensing of Environment 137 (2013) 43–54

Contents lists available at SciVerse ScienceDirect

Remote Sensing of Environment

journal homepage: www.elsevier.com/locate/rse

Detecting continuous lichen abundance for mapping winter caribou forage at landscape spatial scales

Peter R. Nelson [a,c,*], Carl Roland [a], Matthew J. Macander [b], Bruce McCune [c]

[a] Denali National Park and Preserve, P.O. Box 9, Denali Park, AK 99755, USA
[b] ABR, Inc., Environmental Research & Services, P.O. Box 80410, Fairbanks, AK 99709, USA
[c] Department of Botany and Plant Pathology, 2082 Cordley Hall, Oregon State University, Corvallis, OR 97331, USA

ARTICLE INFO

Article history:
Received 4 January 2013
Received in revised form 7 May 2013
Accepted 11 May 2013
Available online 29 June 2013

Keywords:
Lichen
Cladonia
Usnic acid
Spectral
Rangifer tarandus
Forage
Mapping
Landsat 7

ABSTRACT

Spatial variation of available food resources can be difficult to accurately quantify for wide ranging organisms at landscape scales. Lichens with usnic acid, a yellowish pigment, constitute a large portion of caribou winter diet across much of their range. We take a new approach of modeling lichen abundances by capitalizing on unique spectral characteristics of usnic acid lichens. We utilize a recently completed ground reference vegetation data set extending over 12,000 km^2 in Denali National Park and Preserve, Alaska to model the abundance of usnic lichen and other forage vegetation groups. Spectral signatures were obtained for more than 700 vegetation monitoring plots in Denali from Landsat 7 ETM + imagery. We fit models of the absolute percent cover of vegetation groups corresponding to caribou diet items, with a focus on lichens. We used non-parametric multiplicative regression to capture the non-linear relationships between vegetation cover and spectral and environmental data. Different groupings of lichen cover were tried as response variables in addition to usnic lichens to see if other lichen color groups were more detectable. The best fitting lichen model was for usnic acid lichens, which explained 37% of the variation using only three predictors (elevation, bands 1 and 7). Elevation had a non-linear, double-humped shaped relationship to usnic lichen abundance while bands 1 and 7 were positively correlated with usnic lichen cover. These results support previous spectroradiometric ground measurements that indicated usnic lichens were distinctive at those wavelengths. Other vegetation groups had models that explained between 31% and 51% of the variation in cover. Maps of estimated abundance of usnic lichens and other vegetation groups covering the northern half of Denali were generated using our models. These maps enable the study of the role of food resources as a continuous resource in winter habitat selection by caribou, rather than assuming food as a coarser, categorical or thematic variable assigned to discrete areas of the landscape as has been done in most previous studies.

1. Introduction

It is difficult to conduct detailed habitat studies of highly mobile terrestrial species whose individuals range over large areas in a single year. To do so, relevant habitat characteristics must be measured over a wide spatial extent at sufficient resolution to be biologically meaningful. Caribou (*Rangifer tarandus*) are excellent study organisms in this respect. They are also of central importance for subsistence for many human populations across the northern latitudes, both as wild game and domestic livestock. Caribou have large home ranges, in some cases migrating over thousands of miles in a single year (Russell et al., 1993). Caribou respond to many habitat factors but we focused on one, the abundance of winter food resources at landscape spatial scales. Caribou need more energy in the winter due to cold temperatures and difficulty of travel and foraging in snow. Wintering areas therefore often have higher forage abundance (e.g., Johnson et al., 2000). Most caribou subspecies are similar in that their winter diet is composed mostly of lichens, often in the genus *Cladonia*, a terrestrial fruticose macrolichen common across the high northern latitudes (Heggberget et al., 1992; Joly et al., 2007; Russell et al., 1993). Increased soil temperatures in northern latitudes are thought to have caused a decrease in lichen cover caused by tree and shrub expansion (ACIA, 2005; Cornelissen et al., 2001). We need new tools for measuring large-scale woody plant encroachment into lichen-rich areas that are critical to caribou diet during the winter. Such tools would allow us to detect possible changes in forage resources as well as gain a better understanding of caribou ecology. This paper presents a method to make continuous vegetation maps for caribou to meet this need.

Some lichens are distinguishable from other elements of the vegetation using remote sensing data, including use of Normalized

* Corresponding author at: Department of Botany and Plant Pathology, 2082 Cordley Hall, Oregon State University, Corvallis, OR, 97331, USA. Tel.: +1 541 231 5584.
E-mail addresses: peter.ross.nelson@gmail.com (P.R. Nelson), carl_roland@nps.gov (C. Roland), mmacander@abrinc.com (M.J. Macander), Bruce.McCune@science.oregonstate.edu (B. McCune).

0034-4257/$ – see front matter © 2013 Elsevier Inc. All rights reserved.
http://dx.doi.org/10.1016/j.rse.2013.05.026

Difference Vegetation Index (NDVI) (Stow et al., 1993). Many lichen species, including *Cladonia*, are lighter colored and reflect more light in blue to yellow wavelengths than green vegetation, helping to distinguish them from other vegetation (Petzold & Goward, 1988). *Cladonia* species eaten by caribou also commonly contain usnic acid, a pale yellow pigment that is spectrally distinct and has been suggested as a potentially useful characteristic in remote sensing (Petzold & Goward, 1988; Rees et al., 2004). However, no study has focused on the continuous mapping of usnic lichens using remotely sensed data.

Previous studies of caribou habitat incorporated food items by mapping them using remote sensing alone or in combination with other methods (Bechtel et al., 2002; Gilichinsky et al., 2011; Nordberg & Allard, 2002; Petzold & Goward, 1988; Théau et al., 2005). Caribou select food resources at multiple scales (Johnson et al., 2004; Mayor et al., 2009) but most previous studies of caribou habitat that include forage used thematic maps (e.g., categories of % lichen) rather than continuous measures of forage. This approach may be too coarse-grained to detect multiple spatial scales at which caribou are selecting habitat based on food resources if these themes mask important variation in forage. We seek to produce continuous estimates of food resources to enable study of caribou forage resources across multiple spatial scales.

Caribou habitat studies using spectral data fall into three categories: classification, inversion and regression. Classification finds groups of pixels with consistent spectral signatures and assigns a vegetation type to those areas based on reference vegetation data (Jensen, 2005). Classification is useful because it maximizes the purity of spectral signatures of each vegetation type by searching through homogenous pixel areas to gather a larger sample from which to calculate mean spectral characteristics. Inversion solves an equation for the observed reflectance across all bands in a pixel, assuming the spectroradiometric properties of pure pixels for each surface are known (e.g., Hoge & Lyon, 1996; Schlerf & Atzberger, 2006). A successful reflectance model estimates the quantity of each component surface contributing to the reflectance in each pixel. However, pure pixel characteristics for all vegetation types and surfaces in a scene are rarely known. Backscattering, which has been shown to significantly alter spectral signatures of lichens at different illumination angles (Kaasalainen & Rautiainen, 2005), further complicates reflectance modeling. Spectral signatures can be obtained by taking field measurements for all surfaces with field spectroradiometers. However, the potential number of surfaces with unique spectral characteristics and angles of illumination for each can be prohibitively large. We took the third approach, in which we regressed the abundance of vegetation cover groups against spectral and environmental data. Regression enables targeted modeling of spectrally heterogeneous surfaces without having to explicitly account for reflectance properties of other surfaces, as in inversion (Oltof & Fraser, 2007). Regressions can estimate continuous quantities of a target surface within a mixture of co-occurring surfaces, unlike classification, which produces categories of abundance for a target surface. Both of these attributes of regression made it preferable over inversion or classification since we sought to make models and maps of continuous cover for specific vegetation groups.

We seek to map the continuous abundance of major caribou diet categories, especially lichens, by using a large sample of vegetation plots as ground reference data to which we compare the spectral signatures of the same plots. The resulting models and maps will help scientists better quantify food resources for caribou, assess threats to caribou habitat and analyze habitat selection patterns across their range.

Our specific goals are to:

1) Create models to estimate the continuous cover of selected groups of lichens in relation to spectral and environmental data. Lichen groups were: total lichen, usnic lichens (usnic), light-colored lichens (light), usnic plus light colored lichens (usnlite) and dark colored lichens (dark).
2) Create models to estimate the continuous cover of other important caribou diet categories (coniferous and deciduous trees, shrubs and graminoids) using spectral and environmental data as predictors.
3) Estimate the continuous cover of each lichen and vegetation group in areas not directly measured by ground observation (generate maps).
4) Discuss the best predictors in each model and spatial patterns in each map in terms of known ecological and reflectance properties of each lichen and vegetation group.

2. Methods

2.1. Study area

Denali National Park and Preserve (henceforth "Denali"), located in central Alaska (Fig. 1A), covers slightly more than 2.4 million ha between 62° 18′ and 64° 04′ N and between 148° 48′ and 152° 52′ W. Our study area lies in the northern portion of the park covering 1.28 million ha. The Alaska Range, North America's highest mountains, bisects Denali along a northeast/southwest line. North of the Alaska Range is a predominantly continental climatic regime influenced by polar air masses. Vegetation in Denali varies from boreal forests and taiga at the lowest elevations (ca. 100 m), shrublands at middle elevations, and alpine tundra at higher elevations up to the rock and ice zone, which extends to the summit of Mt. McKinley (5934 m; Fig. 2). In Denali, ground dwelling lichens are most abundant in alpine tundra, windswept ridges or lowland open conifer forests but can occur in most habitats except for dense, broadleaf forests or alder thickets. Permafrost occurs sporadically in Denali, from discontinuous patches in mid-elevations to continuous polygons in lower elevations in poorly drained soil types.

2.2. Response data

Response variables were the percent cover of vegetation cover groups, based on data acquired from the National Park Service vegetation monitoring program (Roland et al., 2004). These vegetation cover groups corresponded to categories commonly used by caribou biologists to study diet, including shrubs, graminoids, lichens, deciduous and coniferous trees (Heggberget et al., 1992). Forbs were excluded because we focused on winter diet. We further divided lichens into color groups, partially based on Rees et al. (2004) including yellow colored lichens with usnic acid, such as *Cladonia arbuscula* (Table 1), light colored lichens, such as *Cladonia rangiferina* (Table S1), usnlite (yellow + light) and dark colored lichens, such as *Peltigera aphthosa* (Table S2a–c). We expected lighter colored lichens to be more detectable than dark lichens but also wanted to see if light lichens were spectrally similar enough to usnic lichens to be lumped with them. We therefore also tried the combination of usnic plus light-colored lichens (usnlite) as a response variable. Usnic lichens are yellow in color, light lichens white or gray colored and dark lichens are brown or black. The lichen color categories are mutually exclusive, except for usnlite lichens, which contain both yellow and light color lichens. Usnic lichens are listed in Table 1.

The vegetation monitoring sampling design used a 100 m grid overlaid on Denali based on a random starting position (see Roland et al., 2012). Plots were positioned on the original 100 m grid in groups of 25, called mini-grids (Fig. 1C). Each mini-grid was separated from the next by 20 km (Fig. 1B). Mini-grid spacing was decreased from 20 km to 10 km among-grid spacing in two areas of the park: 1) a 6 km buffer along the park road (which increases ease of access and decreases logistical costs); and 2) in the vicinity of the Toklat basin ecoregion (as a baseline for an area into which a road was being proposed at one time). Within each mini-grid, plots were positioned 500 m apart in each cardinal direction (e.g., every 5th 100 m point) (Fig. 1C). Each plot was a 16 m diameter circle

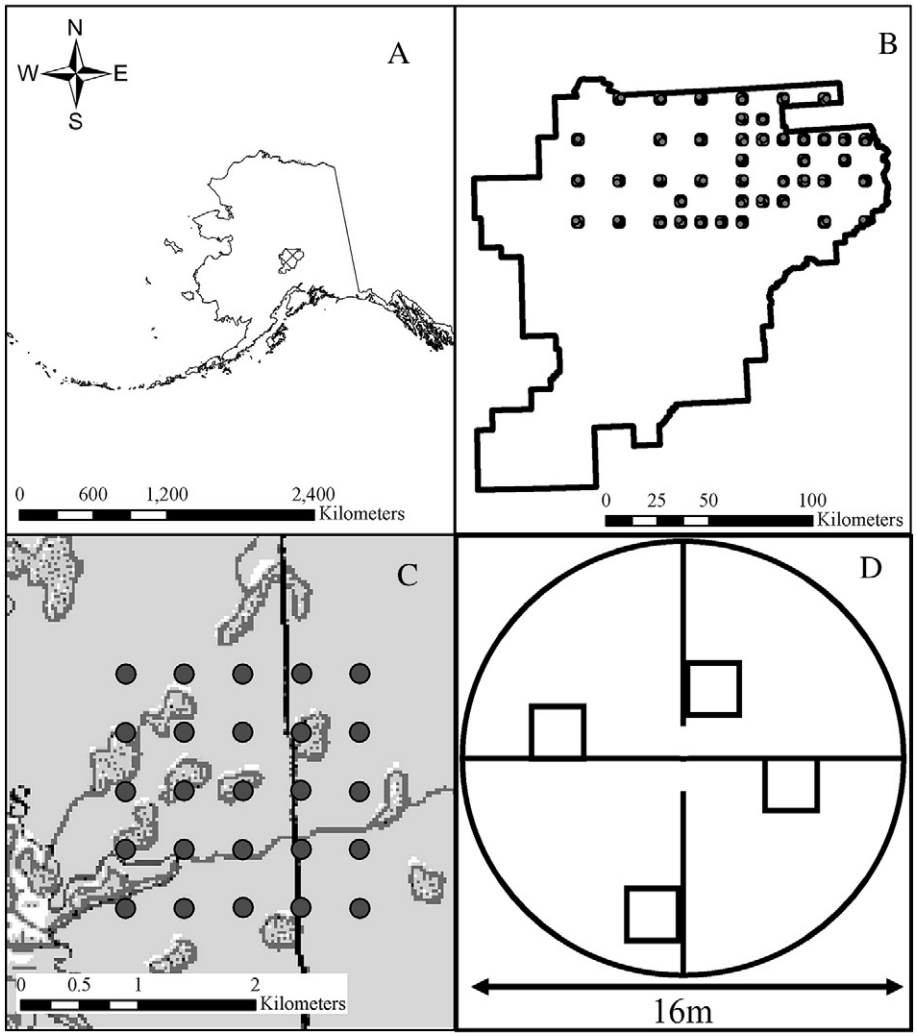

Fig. 1. Maps of nested sampling design for vegetation monitoring in Denali: A) outline of the Park in Alaska B) all mini-grids of vegetation monitoring plots used in this study C) a single mini-grid of vegetation monitoring plots and D) a single plot showing positions of quadrats (squares) and transects (cross lines in circle).

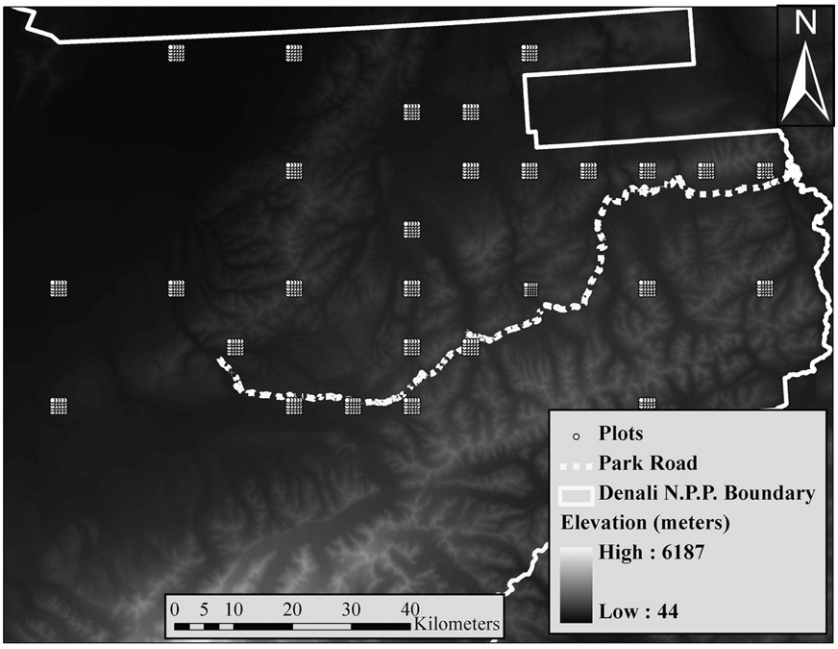

Fig. 2. Elevation map of Denali National Park and Preserve.

Table 1
Abundance and frequency of usnic lichen species found on 722 vegetation monitoring plots in Denali. Mean cover (%) for lichen species used for modeling was calculated as the mean from four 1 m^2 quadrats per plot which was then averaged across all 722 plots. Maximum cover (%) is the highest average cover on a plot. Frequency is the proportion (0–1) of plots that each lichen occurred in. Total cover is the sum of averages by species from all 722 plots. Species are listed in a decreasing order of total cover.

Lichen species	Mean cover	Max cover	Frequency	Total cover
Cladonia arbuscula	0.39	30.25	0.44	562.19
Cladonia amaurocraea	0.29	10.25	0.49	212.44
Nephroma arcticum	0.18	18	0.11	129.06
Cladonia stellaris	0.17	34.56	0.1	121.31
Flavocetraria cucullata	0.16	3	0.44	113.5
Cladonia uncialis	0.09	11	0.15	65.7
Flavocetraria nivalis	0.04	11.56	0.09	30.31
Cladonia mitis	0.03	16.25	0.02	21.69
Dactylina arctica	0.02	1.75	0.12	18.01
Alectoria ochroleuca	0.02	9.56	0.04	16.89
Cladonia deformis	0.02	2	0.14	15.81
Cladonia cyanipes	0.02	0.5	0.19	14.19
Cladonia borealis	0.01	1.06	0.08	8.56
Parmeliopsis ambigua	0.01	0.25	0.1	8.39
Cladonia botrytes	0.01	0.56	0.07	7.68
Asahinea chrysantha	0.01	1.62	0.03	6.38
Arctoparmelia separata	0.01	1.5	0.02	6.12
Cladonia carneola	<0.01	0.5	0.04	3.5
Cladonia pleurota	<0.01	0.88	0.04	3.12
Cladonia sulphurina	<0.01	0.31	0.04	2.69
Arctoparmelia centrifuga	<0.01	1.5	<0.01	2.62
Cladonia bacilliformis	<0.01	0.25	0.03	2.19
Flavocetraria miniscula	<0.01	0.25	0.02	1.56
Cladonia metacorallifera	<0.01	0.19	0.01	1
Cladonia coccifera	<0.01	0.25	0.01	0.94
Arctoparmelia incurva	<0.01	0.5	<0.01	0.56
Cladonia transcendens	<0.01	0.12	0.01	0.5
Cladonia bellidiflora	<0.01	0.06	<0.01	0.12

(Fig. 1D). Although each mini-grid had a maximum of 25 plots, some mini-grids had fewer than 25 plots worth of data due to sampling inaccessibility (plots landing in lakes, on a cliff face, etc.). Plots were sampled between 2002 and 2008.

The abundance of vascular vegetation cover groups (shrubs, graminoids, deciduous and coniferous trees) was measured by point intercept along two perpendicular transects (Fig. 1D), one 16 m long running east to west and the other segmented into two 6 m long segments oriented north to south. Plant species presence was recorded at each intersection of the transect and an imaginary line extended vertically from the ground to infinity. Transects were read in three different horizontal spacing categories (30, 40 or 50 cm) depending on the stature of the vegetation. For example, for plots in forests, 50 cm spacing was used whereas in alpine tundra, a 30 cm spacing was used. The abundance of each plant species was calculated as the percentage of the transect points where each species was present at any vertical stratum directly above the transect tape (absolute percent cover). Absolute percent cover was then aggregated for all plant species in a diet category. Lichen cover at the species level was estimated in a series of four 1 m^2 quadrats per plot (Fig. 1D), which were averaged over the plot to yield a percent cover by lichen species by plot. Quadrats were located in the same position on each plot relative to the plot center. Mean cover by lichen color group was calculated by summing the average cover for all lichens in a given color group. Total lichen cover was measured on the transects because that method sampled a larger area. Lichens were not identified on the transects.

Transect data came from 853 plots from 44 mini-grids, after excluding plots with inadequate or missing spectral data (see Predictor Data Section 2.3). These data included coniferous and deciduous trees, shrubs, graminoids and total lichen. Coniferous tree species cover were almost entirely *Picea glauca* and *Picea mariana*, which was treated as a single group (*Picea*). A third conifer, *Larix laricina*, is deciduous and contributed very little to the total cover of coniferous trees and was therefore excluded. Deciduous tree cover was composed of *Betula neoalaskana*, *Populus balsamifera* and *Populus tremuloides*. Shrubs include dwarf shrubs (*Empetrum*, *Dryas*, *Cassiope*, *Salix* and others) and tall shrubs, including deciduous (*Betula*, *Salix*, *Alnus* and others) or evergreen shrubs (*Ledum*, *Juniperus* and others). Graminoid cover was predominantly sedge species (*Carex* and *Eriophorum*) and a variety of grass genera.

Quadrat data for lichen color groups came from 725 plots from 41 mini-grids. Plots lacking adequate spectral data (see Predictor data Section 2.3) were excluded. The lichen specimens from four mini-grids were not identified in time for this analysis due to budget and schedule constraints, which excluded an additional 90 plots. Upon review of the taxonomic determinations of lichens made by one observer, we determined that quadrat data from 38 plots visited by this individual were unreliable for detailed analysis. However, transect data from this set of plots were usable because no taxonomic errors were detected for vascular plants, which were collected by a different observer. A total of 277 macrolichen species were found on the 725 plots. Each of these species was coded by color corresponding to spectral groups based on Rees et al. (2004). We did not group *Stereocaulon* sp. with usnic lichens like Rees et al. (2004) because *Stereocaulon* lacks usnic acid and we specifically wanted to test the detectability of usnic lichens. The 725 plots contained 28 lichen species with usnic acid. The seven most abundant usnic lichens (>0.03% average cover) were, from most to least abundant: *C. arbuscula*, *Cladonia amaurocraea*, *Nephroma arcticum*, *Cladonia stellaris*, *Flavocetraria cucullata* and *Cladonia uncialis* (Table 1). All four *Cladonia* species in this list are important caribou winter forage.

Our plots were much smaller than the area covered by a Landsat pixel. To be sure we had an adequate signal/noise ratio to use plots as our sample units for quadrat-level data (usnic, usnlite, light and dark lichens), we verified that between-plot variation in lichen cover was greater than within plot variation. ANOVA of quadrat lichen cover ($n = 2368$ quadrats) with plot ($n = 592$) as a factor showed more variation in lichen cover between plots than between quadrats within plots, with a signal/noise ratio of five ($F = 5.03$, $df = 591$, $p < 0.0001$).

2.3. Predictor data

We obtained plot spectral characteristics from two scenes (August 16, 2000) from the Landsat 7 ETM+ sensor (Path 70/Rows 15 and 16). The 30 m pixels (bands 1/2/3/4/5/7) for the two scenes were calibrated to top-of-atmosphere reflectance (TOA) (Chander et al., 2009). The reflectance values (0–1.0) were scaled by 10,000 and stored as signed integers. The two scenes were mosaicked together and then clipped to a bounding box defined by the border of Denali plus a 16 km buffer.

Denali contains extensive areas of hilly and mountainous terrain, where these topographic effects on remote-sensing imagery are most pronounced. Sun angles are low at high latitudes, which further increase topographic effects. To minimize these effects, we normalized illumination and corrected for backward radiance (Colby, 1991) using a Minnaert correction (Smith et al., 1980). The Minnaert correction model is expressed as:

$$\rho_H = \rho_T * \cos\ e/(\cos\ e\ \ \cos i)^k \quad (1)$$

where ρ_H is the equivalent reflectance on a flat surface with incident angle of zero, ρ_T is the observed reflectance, e is the terrain slope, i is the solar incidence angle (the angle between the terrain normal and the solar radiation) and k is the Minnaert value (Table 2). The cosine of the solar incidence angle ($\cos i$) is calculated as:

$$\cos i = \cos\theta\ \ \cos e + \sin\theta\ \ \sin e\ \ \cos(\varphi_m - \varphi_s) \quad (2)$$

Table 2
Minnaert *k* values used for incidence angle correction (Macander, 2010).

Band	*k*
1	0.226
2	0.416
3	0.555
4	0.577
5	0.71
7	0.825

where θ = solar zenith angle, φ_s = solar azimuth, e = terrain slope and φ_m = terrain aspect. Terrain slope and aspect were calculated from the National Elevation Dataset 2-minute DEM data (resampled to 30 m resolution using bilinear resampling) while solar parameters were obtained from the Landsat metadata. Minnaert *k* values were assigned based on an analysis done for a Landsat mosaic in northwest Alaska with similar land cover types (Macander, 2010). Incident corrected reflectance values were calculated from top of atmosphere reflectance values using Eq. (1).

A 9-pixel (3 × 3 window of 30 m pixels = 8100 m^2) neighborhood centered on each plot was used as the area from which spectral signatures (mean reflectance by band) were obtained. Within each plot's 9-pixel neighborhood, pixels were flagged if they fell in stripes (instrument artifacts), shadow, or very low illumination angles. Plots without complete 9-pixel signatures (containing flagged pixels) were not used in the analyses.

Three plots nearly devoid of vegetation and located on steep slopes were deleted from the pool of plots with quadrat data. They also had abnormally high reflectance across most bands. This was likely caused by the combination of steep slopes and high mineral cover on these plots. The remaining 722 plots with lichen data were used for modeling lichen cover groups based on their cover averaged across quadrats on a plot (see Section 2.2 Response data). Three plots were deleted from the pool of plots with transect data for the same reasons, two of which were the same plots excluded from the pool of plots for the quadrat data, for a total of 850 plots used in plot-level modeling based on transect cover of vegetation groups.

Scatterplots between predictors (spectral and environmental data, Table 4) and the responses (lichen and vegetation data) indicated possible benefits of log transformation of the spectral bands and elevation. Also, as spectral bands are inter-correlated, a principle component analysis (PCA; McCune & Mefford, 2011) was conducted on $\log_{10}$ transformed reflectance values. PCAs were run separately for both pools of plots (quadrat data and transect data, respectively) because the identity and number of plots differed (n = 722 for quadrats vs. n = 850 for transects, see Section 2.2 Response data). PCAs used correlations in the cross-product matrix. Eigenvectors for both PCAs are in Table 3. Scores of plots on all 6 axes (principal components) are orthogonal, linear composites of the bands. All PCA axes were retained because any axis was a potentially informative predictor of vegetation. Relationships between the abundance of vegetation groups in spectral space were also visually assessed using symbol-size overlays in PC-ORD (McCune & Mefford, 2011) (Fig. 3). Normalized Difference Vegetation Index (NDVI) was calculated using the $\log_{10}$ transformed bands (LNDVI) to maintain comparability between the scales of the spectral predictors. LNDVI is strongly correlated (R^2 = 0.96) with NDVI and can be interpreted in the same way as NDVI.

In addition to the spectral data, environmental variables from each plot were included in the predictor matrix. The non-spectral variables were added to the predictor matrix to account for environmental gradients known to influence the abundance of vegetation groups but not necessarily captured by spectral variables. Environmental data collected on the plot used for modeling include slope, aspect and elevation. Derivations of these environmental data also added to the predictor matrix include aspect off 180°, equivalent latitude,

Table 3
Principal components used to extrapolate relationships of vegetation to spectral data. To apply eigenvectors to new values, the bands are first log transformed, then variable's mean is subtracted and divided by the corresponding standard deviation. Note the naming convention LPCA is used for both lichen and veg data sets but sample sizes differed (n = 722 for lichen data, n = 850 for veg data) between PCAs. LICB stands for "$\log_{10}$ incident corrected band".

PCA data sets and statistics	LICB1	LICB2	LICB3	LICB4	LICB5	LICB6
Plots with lichen data						
Mean	2.997	2.959	2.848	3.513	3.311	2.964
Standard deviation	0.034	0.055	0.096	0.099	0.115	0.128
Eigenvectors						
1	−0.381	−0.457	−0.453	−0.232	−0.421	−0.458
2	−0.491	−0.152	−0.242	0.726	0.379	0.084
3	0.286	0.426	−0.031	0.535	−0.379	-0.553
4	0.700	−0.327	−0.587	0.091	0.206	0.090
5	0.203	−0.665	0.624	0.207	0.062	−0.284
6	−0.032	0.193	−0.041	−0.288	0.700	−0.623
Plots with veg data						
Mean	2.998	2.959	2.847	3.508	3.302	2.956
Standard deviation	0.041	0.062	0.106	0.109	0.126	0.136
Eigenvectors						
1	−0.383	−0.471	−0.472	−0.186	−0.394	−0.468
2	0.470	0.205	0.241	−0.661	−0.456	−0.187
3	−0.204	−0.408	0.024	−0.633	0.317	0.539
4	0.739	−0.288	−0.569	0.078	0.190	0.067
5	0.206	−0.662	0.626	0.185	0.097	−0.290
6	−0.047	0.223	−0.051	−0.295	0.701	−0.606

PDIR (Potential Direct Incident Radiation) and heatload. The aspect off 180 (degrees away from south) was calculated in a database, equivalent latitude (Dingman & Koutz, 1974) calculated in R and PDIR and heatload (McCune, 2007) calculated in HyperNiche (McCune & Mefford, 2009). Geologic environmental variables included in the predictor matrix were extracted from GIS layers (1:250,000 scale) based on the Denali soil survey (Clark & Duffy, 2006), including permafrost, lithology (surficial geology), parent material, landform and ecoregion subsection (Table S3). We collapsed the ecoregion subsection from eighteen down to eleven classes to reduce the number of categories. We also used fire year as a predictor, which was obtained from the NPS Alaska Region Fire perimeter GIS layer (1:63,360 scale) and calculated as year of the Landsat scene (2000) minus the fire year plus 1 year. Fires were assigned "1" that occurred the same year but before the day the Landsat scene was acquired. These environmental variables were rasterized to 30 m pixel grain to match the Landsat image so that they could be used in generating maps (see Section 2.5 Outputs). A final pool of 25 predictors (Table 4) was used in the regression step detailed in the next section.

2.4. Model type and parameters used

The percent covers of lichen and vegetation groups (dependent variables) were regressed against the spectral and environmental predictor variables (independent variables; Table 4) with non-parametric multiplicative regression (NPMR) (McCune, 2006) in the program HyperNiche (McCune & Mefford, 2009). NPMR can recover complex unanticipated nonlinear response surfaces and automatically represents interactions among predictors using multiplicative weights with a kernel smoother. We used NPMR with a Gaussian kernel and forward stepwise variable selection, simultaneously optimizing the smoothing parameters (tolerances) for all predictors included in the model. NPMR controls over-fitting with leave-one-out cross validation during model selection and calculating fit so that splitting into training/validation data sets is automatically built into model development.

We set the minimum average neighborhood size for an acceptable model to 10 and the allowable missing estimates for an acceptable model to 3%. The neighborhood size setting means that, on average

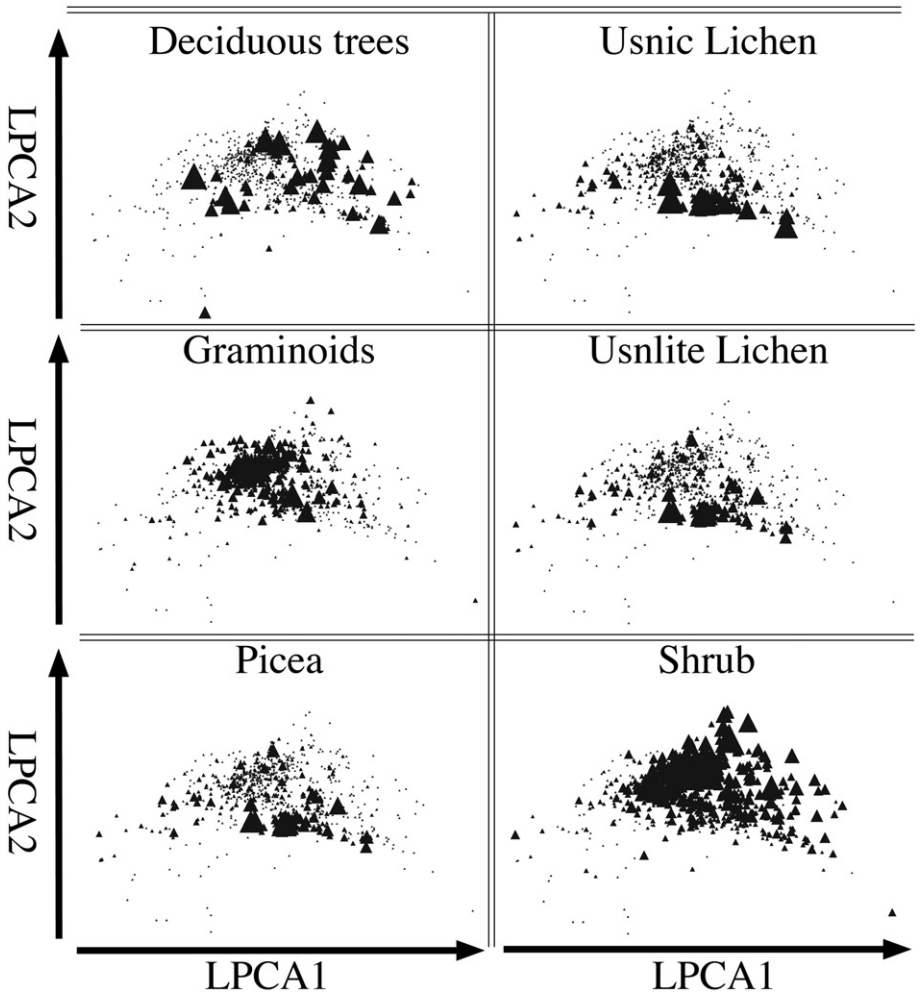

Fig. 3. Abundance of vegetation groups and usnic and usnlite lichens superimposed on the first two principal components (LPCA1 and LPCA2) of 722 plots in spectral space (variables LICB1–5 and 7 in Table 4). LPCA stands for principle component analysis using $\log_{10}$ incident corrected bands. LICB means $\log_{10}$ incident corrected bands. Triangles represent plots and the symbol size is proportional to abundance.

Table 4
List of predictor codes and descriptions for those used in modeling vegetation and lichen cover. NDVI was calculated as (LICB 4–3/LICB 4+3) with $\log_{10}$ transformed bands for the sake of comparability to the other bands. See Section 2.3 predictor data for methods of calculating each predictor. See Table S3 classes of categorical variables.

Predictor code	Predictor description	Units
pslope	Plot slope	Degrees
pelevati	Log_{10} plot elevation	Meters
pequival	Plot equivalent latitude	Degrees
paspecto	Plot aspect off 180	Degrees
LICB1–5 & 7	Log_{10} incident corrected Landsat 7 ETM+ band 1–5,7	Reflectance
LNDVI	Normalized Difference Vegetation Index calculated using $\log_{10}$ transformed bands	Unitless
PDIR	Potential direct incident radiation	Mega joules/cm^2/year
heatload	Heatload	Unitless transformation of PDIR
LPCA1-6	Principle component axes 1–6 using $\log_{10}$ transformed incident corrected bands	Standard deviations from the centroid
litho	Lithography	Categorical
parent	Parent material	Categorical
landfor	Landform	Categorical
perma	Permafrost	Categorical
ecoreg	Ecoregion subsection	Categorical
fireyear	Time since fire	Year

for a given model, the equivalent of 10 or more plots must bear on an estimate for a model to be retained. By using a low allowance for missing estimates we forced the model to maintain adequate spatial coverage; this results in a more conservative model with broader tolerances. Although model fit increases if more missing estimates are allowed, gaps are produced in the maps, which is not desirable for the sake of continuity. Attempts to improve a given model were abandoned when all trial improvements in cross-validated R^2 ($\text{x}R^2$) were less than 1%. This criterion was chosen to prevent addition of variables that made only small improvements to the fit. More parsimonious models are more readily interpreted and result in fewer missing estimates because of insufficient data. This is because each additional predictor narrows the multidimensional window in the predictor space, such that new data points are more likely to have combinations of predictor values that are poorly represented in the calibration data.

The model with the largest $\text{x}R^2$, subject to the overfitting constraints described above, was selected as the best model for each vegetation group. The best model for each vegetation or lichen color group was tuned in HyperNiche, which makes fine adjustments in the tolerances of each predictor. The model with highest $\text{x}R^2$ after tuning was retained as the best model. The relative importance of predictors was evaluated with a sensitivity analysis in HyperNiche. The sensitivity analysis nudges the value of each predictor and

measures the change in the response. Sensitivity to a predictor is a change in the response, measured as a percentage of the range of the response, expressed relative to the magnitude of the change in the predictor. For example, a sensitivity of 0.5 means a 5% change in the predictor causes a 2.5% change in the response. Higher values mean the model is more sensitive to changes in that predictor, which can be interpreted as more importance for that predictor in the model. Sensitivities for models with $xR^2 < 0.2$ were not evaluated.

Finally, for each final model we tested the null hypothesis that the fit is no better than expected by chance alone, based on a randomization test. The probability of Type I error was calculated by refitting the model 100 times after randomizing the rows of the predictor matrix relative to the response variable. The resulting *p*-value is the proportion of models fit to randomized data with the same number of predictors that had as good or better fits than with the nonrandomized data. Models with $xR^2 < 0.2$ were not subject to a randomization test.

2.5. Output maps

Maps of the vegetation groups were generated using the best, tuned model for each respective vegetation group (Table 5). HyperNiche uses a chosen model and rasters of each predictor to make estimates for the response, resulting in an output grid for the response of the same dimensions as the input rasters. Rasters for the predictors of equal spatial coverage and cell size were generated in ArcGIS 9.3.1 (see Predictor data Section 2.3). Rasters of PCA axes were generated from eigenvectors (Table 3) from PC-ORD using the Map Algebra tool in ArcGIS. Finally, output grids from HyperNiche for lichen and vegetation groups were imported into ArcGIS for display as maps.

3. Results

3.1. Lichen group models

Usnic lichens had the best fitting model ($xR^2 = 0.37$) of the lichen groups followed by usnlite lichens, light and dark lichens. Of the lichen groups, only usnic and usnlite lichens had good fitting models ($xR^2 > 0.2$; Table 5). Usnic and usnlite models both included elevation but differed in the spectral and environmental predictors selected (Table 5). In addition to elevation, usnic lichens were related to $\log_{10}$ incident corrected bands 1 and 7 (LICB1 and LICB7). The relationships between the best predictors and usnic lichen cover were nonlinear, with high cover corresponding to areas in low elevations but high reflectance in LICB1 (Fig. 4). The usnic lichen model had sufficient data to make estimates for most of the study area (Fig. 5A). Areas with no estimates include most high elevation rock and ice areas, water bodies and gravel bars. The best usnlite lichen model performed slightly worse ($xR^2 = 0.32$) than the best usnic lichen model. In addition to elevation, the best usnlite lichen model contained landform as well as two spectral predictors (Table 5). The inclusion of landform, a categorical variable, resulted in a less continuous and blockier map for usnlite lichens (Fig. 5B). Dark and light lichen models performed poorly. Both usnic and usnlite models fit significantly better than models fit to 100 randomizations of the original data (Table 5). Although our plots were much smaller than Landsat pixels, we confirmed that there was five times more signal (between-plot variation) than noise (within-plot variation) in our usnic lichen data (see Section 2.3 Predictor data).

3.2. Vegetation group models

Picea had the best fitting model ($xR^2 = 0.53$) of all the vegetation groups followed by shrub, graminoid, total lichen and deciduous tree. The best predictors for *Picea* cover were elevation, $\log_{10}$ incident corrected band 5 (LICB5) and principle components axis 1 (LPCA1, loading most heavily bands 2, 3 and 7) from a PCA of $\log_{10}$ incident corrected bands. The best shrub model had only two predictors, $\log_{10}$ incident corrected band 2 (LICB2) and normalized difference vegetation index calculated from $\log_{10}$ incident corrected bands 3 and 4 (LNDVI), yet a moderately good fit ($xR^2 = 0.4$). The best graminoid model had four predictors (elevation, slope, $\log_{10}$ incident corrected band 3 (LICB3) and ecoregion) that accounted for 31% of the variation. Total lichen had a poorer fitting model accounting for 27% of the variation using elevation and $\log_{10}$ incident corrected bands 3 and 5 (LICB3 and LICB5). Deciduous trees had the poorest fitting model ($xR^2 = 0.24$) with the predictor elevation, $\log_{10}$ incident corrected band 3 (LICB3) and ecoregion. All vegetation cover models beat the randomization test (Table 5).

4. Discussion

4.1. Lichen models — spectral characteristics

Usnic lichens reflect more light at visible to near infra-red wavelengths compared to other lichen or vegetation groups (Fig. 6). This is especially true in band 1 or blue bandpass (450–520 nm) (Petzold & Goward, 1988; Rees et al., 1998), where other lichens and vegetation

Table 5
Best predictors and models for each vegetation and lichen group with model statistics and sample sizes for each data source (quadrat or transect); each column is a model; *p* = proportion of models fit to 100 randomized copies of original data set that were better than original model, xR^2 = cross-validated R^2, RMSE = root mean square error, N-hood = average neighborhood size (sum of weights, number of plots), tol = tolerance is the width of the Gaussian kernel measured as a percentage of the range of the predictor, sens = sensitivity is the percent change in response resulting from 1% nudging of predictor, pred = predictor. Categorical variables have zero tolerance by definition, and were not subjected to sensitivity analysis. "*" indicates sensitivities that weren't calculated because models had a poor fit ($xR^2 < 0.2$). See Table 4 for predictor abbreviation definitions.

Quadrat data (n = 722)					Transect data (n = 850)				
Model stats	Usnic	Light	Usnlite	Dark	Picea	Deciduous tree	Shrub	Graminoid	Lichen
p	0.01	*	0.01	*	0.01	0.01	0.01	0.01	0.01
xR^2	0.37	0.19	0.32	0.11	0.51	0.24	0.4	0.31	0.27
RMSE	2.9	*	6	*	1.57	1.26	3.22	1.41	1.38
N-hood	31.4	23.6	23.2	42	53.3	57.1	83	24.5	63.8
pred 1	pelevati	pslope	pelevati	pelevati	pelevati	pelevati	LICB2	pslope	pelevati
tol. 1	0.05	10.38	0.05	0.05	0.13	0.13	0.02	6.51	0.14
sens. 1	0.23	*	0.23	*	0.08	0.6	0.3	0.11	0.13
pred 2	LICB1	pelevati	LICB2	LNDVI	LICB5	LICB3	LNDVI	pelevati	LICB3
tol. 2	0.01	0.05	0.06	0.01	0.05	0.12	0.01	0.13	0.06
sens. 2	0.23	*	0.05	*	0.32	0.04	0.73	0.1	0.4
pred 3	LICB7	LICB4	landfor	LPCA6	LPCA1	ecoreg	–	LICB3	LICB5
tol. 3	0.11	0.1	0	0.08	0.54	0	–	0.07	0.05
sens. 3	0.08	*	n/a	*	0.45	n/a	–	0.17	0.41
pred 4	–	landfor	LPCA2	fireyear	–	–	–	ecoreg	–
tol. 4	–	0	1.3	8.8	–	–	–	0	–
sens. 4	–	n/a	0.04	*	–	–	–	n/a	–

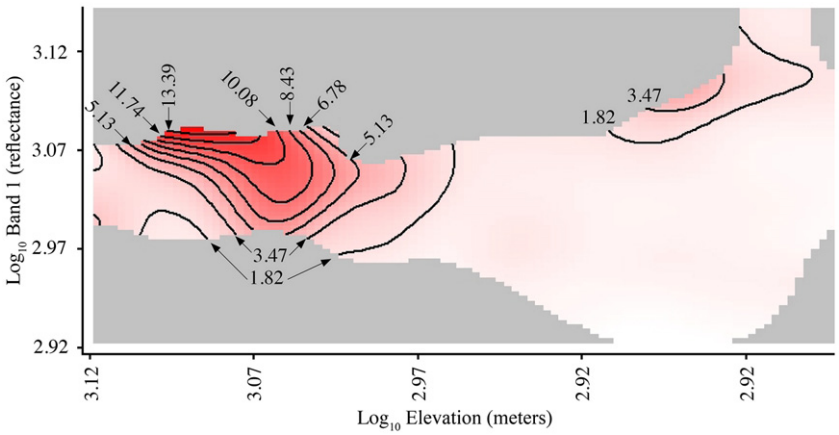

Fig. 4. Contour surface of estimated percent cover of usnic lichens in relation to the two most important predictors (log_{10} incident corrected band 1 and log_{10} elevation) as determined by sensitivity analysis. The 3D surface was based on the tolerances selected for the four-predictor model (Table 5). Gray background indicates areas where the model made no estimate.

absorb strongly (Fig. 6). This explains the positive relationship between usnic lichen abundance and brightness in log_{10} incident corrected band 1 (LICB1) (Fig. 4). Surprisingly, the pale yellow color of usnic lichens did not correspond to a spectral predictor in the models. If the yellow color of usnic acid had been a useful spectral characteristic, then band 2 (green into yellow bandpass, 520–600 nm) would have been included in the models. The breadth of band 2 likely diminishes the signal of yellow wavelengths because the dominant green reflectance of many vascular plants (Fig. 6) dilutes the yellow signal. Furthermore, spectrophotometer trials with pure usnic acid dissolved in acetone showed the spectral signal in the yellow range to be very weak, compared to the peak in UV absorbance.

Both light lichens (e.g., *Stereocaulon paschale* in Fig. 6) and usnic lichens possess much stronger reflectance in green bandpass than other vegetation, which likely explains why log_{10} incident corrected band 2 (LICB2, green bandpass, 520–600 nm) came into the usnlite model. However, adding usnic and light lichens together may have diluted the distinctiveness of usnic lichens in band 1, diminishing the power of the best usnic lichen spectral predictor.

Dark lichens absorb much of the visible electromagnetic spectrum but their reflectance shows a rapid rise and small peak in near-infrared reflectance (Fig. 6) (Petzold & Goward, 1988), which provides a spectral basis for their differentiation. Rocks with and without dark lichens have been successfully differentiated using hyperspectral imagery (e.g., Zhang et al., 2005). However, these features may be too narrow spectrally for the wide bandpass of the sensor used, which may explain the poor fit of the model for this color group.

4.2. Lichen models — ecological and spatial patterns

We found two peaks in usnic lichen abundance in Denali: lowland, largely forested, alluvial terraces and alpine tundra (Fig. 5A). We hypothesize that these peaks in lichen correspond to areas that lack dense woody vegetation and lack deep moss mats, as explained below.

Rockiness is positively related to lichen abundance in the arctic (Holt et al., 2007). Very rocky soils suppress vascular plant cover, favoring lichens and bryophytes. Lichens are poor competitors against vascular plants but tolerate high stress environments where low temperatures and low water availability reduce or exclude vascular plant cover (Grime, 1977). We therefore expect lichens to be most abundant in areas with thin or rocky soils, less conducive to abundant vascular plant cover.

Furthermore, deep moss mat development appears to disfavor lichens. Forests in interior Alaska that have not burned often develop a thick moss mat and spruce overstory that insulates the active layer. Deeper moss furthers the development of permafrost via insulation and favors a bryophyte understory and low lichen abundance (Bonan & Shugart, 1989; Viereck & Schandelmeier, 1980).

Our map shows a large patch of high usnic and usnlite lichen abundance (Fig. 5A and B) in the low elevation spruce forests (Fig. 5C) in the western region of our study area. During field work in this area, we observed very thin, rocky soils on this large alluvial terrace (Clark & Duffy, 2006), which conforms to the idea that lichens are more abundant on less productive, rocky, well-drained soils.

Usnic and usnlite lichen cover was high on alluvial terraces that experienced large fires in 1986, 1990, 1991 and 1993. This development of lichen mats on recent burns conflicts with some prior studies on lichen regeneration after fire (Joly et al., 2009) but is supported by others (Holt et al., 2008). We observed dense lichen mats below burnt *P. glauca* snags amongst widely spaced, younger *Populus* trees that had established post-fire. While fires may reduce lichen abundance in the short term, they may enhance it in the long term, depending on soil characteristics, pre-fire lichen abundance and fire behavior (Kershaw, 1978). When fires remove the dense moss and organic layers there is more substrate available for lichens to colonize, although mosses are often more abundant post-fire in areas of permafrost (Viereck & Schandelmeier, 1980). Fires also favor lichen growth by increasing the amount of light reaching the understory by removing the forest canopy.

Lichen covered ridges are a familiar sight to visitors to the interior of Alaska, where light yellowish lichen-tinted tundra stands out at a distance against the dark green of surrounding forests. These alpine communities with high lichen abundance within the study area are visible on our map as a fine, reticulated higher lichen abundance north and southwest of the end of the park road (Fig. 5A and B). The alpine lichen communities are less pronounced on the map but reflect the same ecological tendency of lichens to be abundant on thin, rocky soils (Ahti, 1977; Bonan & Shugart, 1989; Holt et al., 2007, 2008). In the alpine, cold temperatures due to higher elevations and wind exposure, especially on ridges, suppress large woody plants. This combination of environmental factors allows lichen communities to establish and persist.

4.3. Vegetation models

Two predictors, green bandpass (log_{10} incident corrected band 2 (LICB2), 520–600 nm) and NDVI based on log_{10} incident corrected bands (LNDVI), accounted for 40% of the variation in shrub cover. These predictors correspond to the reflectance features of shrubs; in particular, the reflectance profile of the common and abundant shrub *Betula glandulosa* (dwarf birch) peaks in bands 2 and band 4

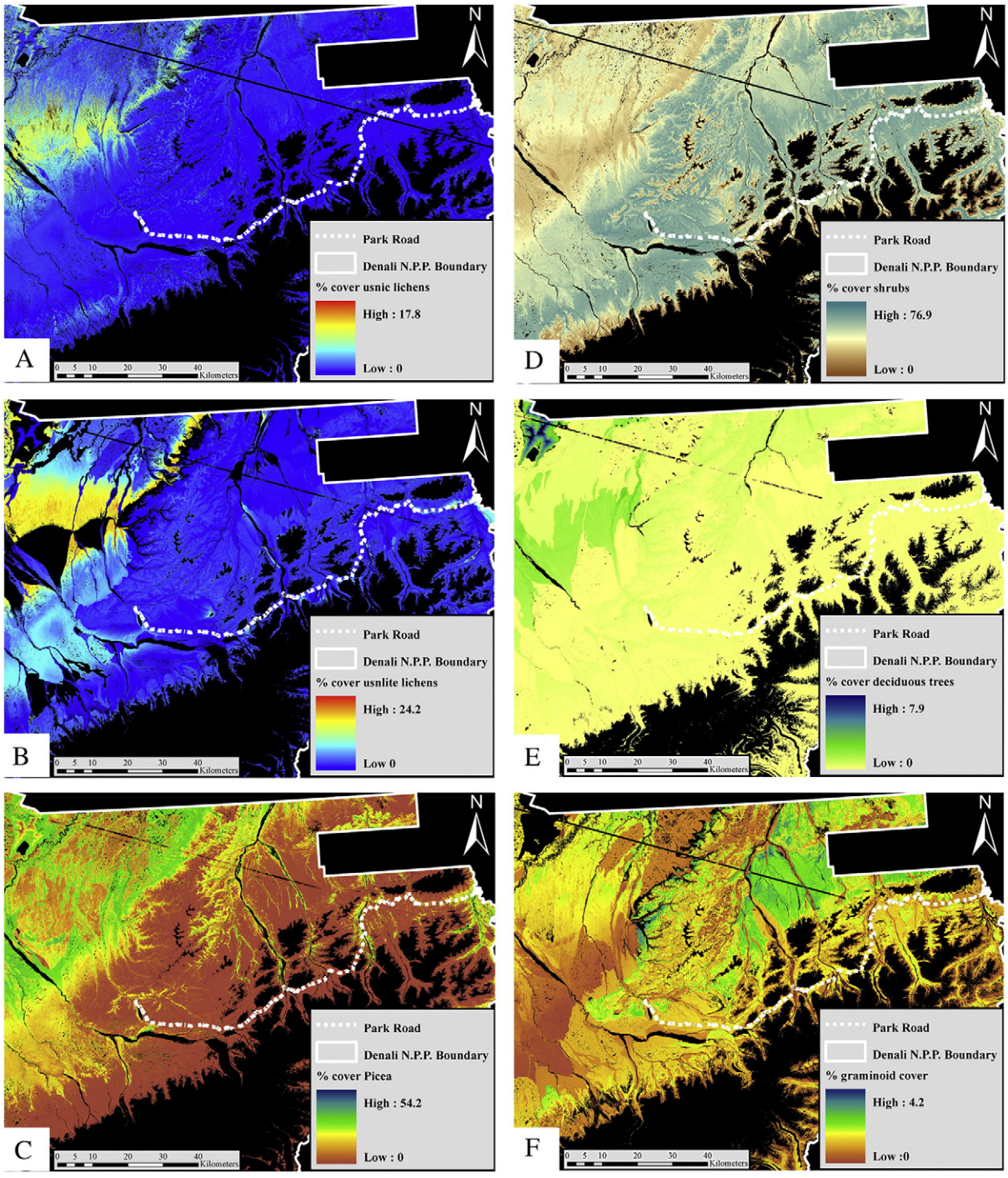

Fig. 5. Maps of the estimated cover of vegetation groups and usnic and usnlite lichens in Denali. Cover estimates were generated using models of spectral and environmental characteristics of the vegetation monitoring plots: A) usnic lichens B) usnlite lichens C) *Picea* sp. D) shrubs E) deciduous trees and F) graminoids. Black areas inside Denali's border had no estimate made for the vegetation group because of too few plots that were sampled on sites with those spectral and environmental characteristics.

relative to band 3 (Fig. 6). The resulting shrub map shows a broad swath of high abundance in mid-elevations along the north slope of the Alaska Range (Fig. 5D). This pattern is largely driven by dwarf birch and *Alnus viride* (alder). Alder is found in steep or wet areas lacking permafrost, whereas dwarf birch tends to occupy colder soils (Viereck et al., 1992).

In our models, *Picea* cover is strongly related to elevation because factors such as soil moisture, permafrost, and temperature, among others, which have been shown to control tree patterns at a landscape-scale in Denali, also change with elevation (Roland et al., 2012; Stueve et al., 2010). Areas of high *Picea* cover in Denali all occur north of the Alaska Range where elevations fall below 600 m (Fig. 5C). In contrast, most of the middle elevation areas have sparse conifer cover and abundant shrubs (Fig. 5D). The broad swath of high *Picea* cover at low elevations corresponds to either taiga dominated by *P. mariana* in areas of cold, wet soils on permafrost or *P. glauca* in well-drained, warmer soils or riparian areas thawed by moving water (Roland et al., 2012). Abundance of *Picea* is negatively related to $\log_{10}$ incident corrected band 5 (LICB5). Other authors have also found low reflectance in the near infra-red to be a

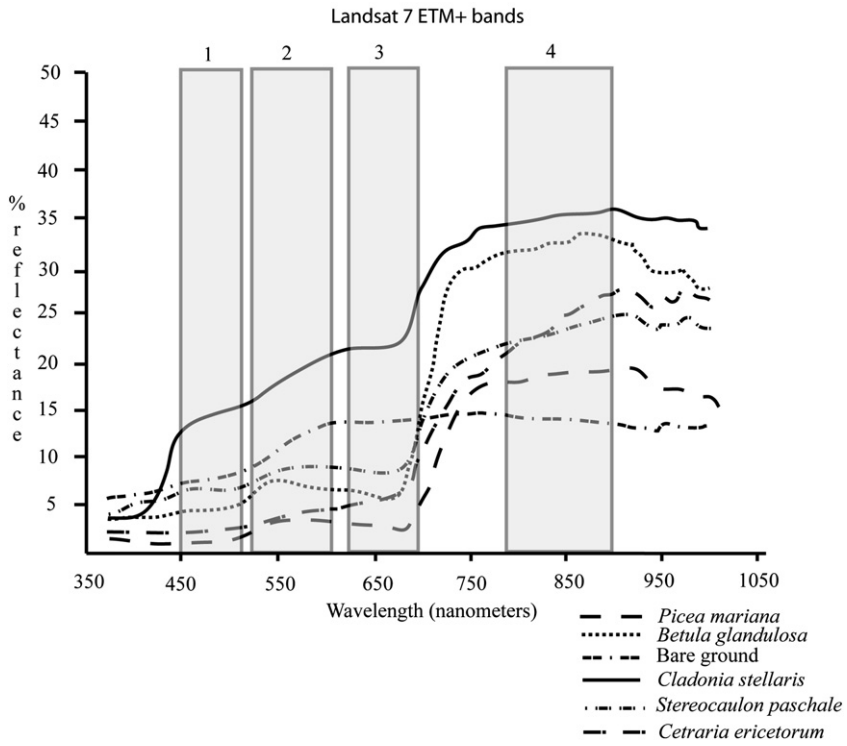

Fig. 6. Mean reflectance profiles of plant and lichen species belonging to vegetation cover groups used here. *P. mariana* = *Picea*, *Betula glandulosa* = shrub, *Cladonia stellaris* = usnic lichens, *Stereocaulon paschale* = light lichens, *Cetraria ericetorum* = dark lichens. Spectral profiles were not reported beyond 1050 nm in original publication. Data adapted from Petzold and Goward (1988). Gray bars indicate the bandpasses for the first four bands in the Landsat 7 ETM + sensor.

good predictor of high conifer cover (Horler & Ahern, 1986). PCA axis 1 based on $\log_{10}$ incident corrected bands (LPCA1) also came into the *Picea* model and is strongly loaded with bands 1, 2 and 3. LCPA1 was likely selected as a predictor of *Picea* because *Picea* strongly absorbs energy in bands 1 and 3 (Fig. 6), relative to other vegetation and lichen groups. *Picea* abundance is more sensitive to the spectral predictors than elevation (Table 5), so small variations in LICB5 and LPCA1 across the Landsat scene allowed the model to successfully recover several small conifer patches, such as those south of Wonder Lake just south of the western end of the park road (Fig. 5C).

Despite the relatively poor fit of the deciduous tree model (xR^2 = 0.24), it successfully detected the large patch of forest, primarily *B. neoalaskana*, in hills around Lake Chilchukabena in the northwest corner of the map (Fig. 5E). This area has well-drained, warmer, mineral soils, much of which burned 44 years ago. Fire increases deciduous tree abundance in Denali (Roland et al., 2012). However, fire (as years since burn) did not enter the model, possibly because too few plots occurred in dense broadleaf forests, which are relatively rare in this landscape (Roland et al., 2012). The model also correctly mapped *Populus* forests in the west central portion of the map (Fig. 5E), corresponding to conifer forests on alluvial terraces that burned 10–15 years ago and regenerated as deciduous forests. This is noteworthy in part due to the rarity and patchiness of *Populus* occurrence in Denali (Roland et al., 2012). Both of these high deciduous tree cover areas fall within two ecoregion subsections (low mountain and alluvial terraces, respectively), explaining why the ecoregion subsection came into the model as a predictor. Like our *Picea* model, elevation was the single best predictor for deciduous trees because it is correlated with factors such as temperature that control tree establishment and growth in this area (Roland et al., 2012). Log_{10} incident corrected band 3 (LICB3, red bandpass, 630–690 nm) was negatively related to deciduous tree cover. Another study mapping broadleaf tree cover also found a negative relationship between cover and red bandpass (Franklin et al., 1991), although the physical mechanism for this was not stated.

Slope was the best predictor of graminoid cover, reflecting the tendency of graminoids to occur in flat areas in Denali. Elevation has a more complex, non-linear relationship to graminoid cover, since some uplands have abundant grasses and sedges. However, the highest graminoid cover in Denali tends to be tussock tundra and muskeg in low to mid elevations dominated by two species, *Eriophorum vaginatum* and *Carex bigelowii*. The Toklat basin ecoregion subsection is one such area, depicted as a roughly circular feature of high graminoid cover in the north central portion of Denali (Fig. 5F). Since it is its own ecoregion subsection and has such high graminoid cover, the Toklat basin likely influenced ecoregion subsection to come in the graminoid model. NDVI has a positive relationship with graminoid cover (Riedel et al., 2005) but did not enter the model. Instead, only a component of NDVI, $\log_{10}$ incident corrected band 3 (LICB3, red bandpass), was selected as a good spectral predictor, which had a unimodal or hump-shaped relationship to graminoid cover. Graminoids generally co-occur with other plants with a stronger relationship to NDVI (shrubs), which may partially explain why NDVI didn't come into the graminoid model. Also, the graminoid tussocks have many shadows and may have a very large standing dead/litter component. Much of the graminoid may have also senesced by Aug. 16 when the Landsat scene was acquired. Shadow, litter or senesced leaves would dilute the positive relationship between NDVI and graminoids and combined, may explain why NDVI failed to come into the model.

5. Conclusions

Other studies have estimated the cover of groups of forage lichens that included those with usnic acid (Nordberg & Allard, 2002; Théau et al., 2005). However, this is the first study to focus on modeling usnic lichens to estimate their landscape-scale abundance. Usnic lichen cover is positively correlated with total lichen cover (Fig. 7). Caribou also consume light and dark lichens, making usnic lichens a useful tool for mapping total lichen cover. Models could be improved

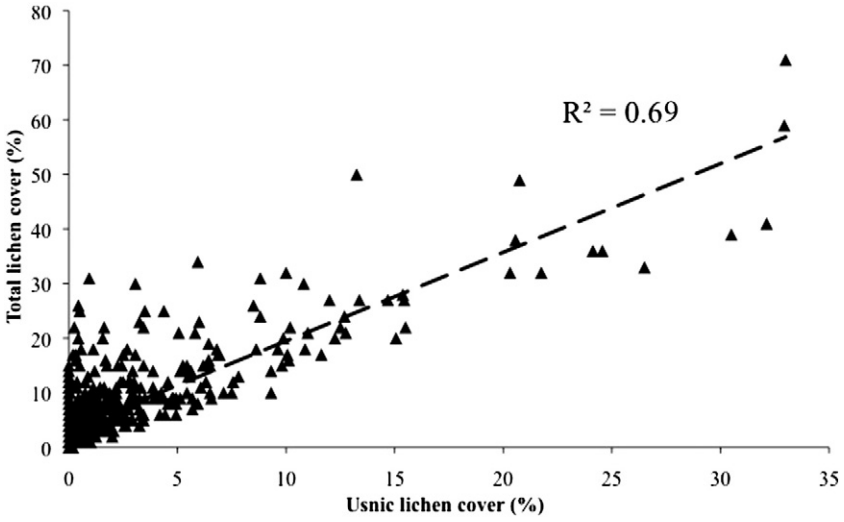

Fig. 7. Scatterplot of total lichen cover versus total usnic lichen cover from 722 plots. Both lichen cover estimates are averaged over four quadrats per plot. Triangles represent plots.

by increasing the number of quadrats sampled for lichens at each plot and increasing plot size relative to image pixel size. Repeating these analyses with finer grained, hyperspectral products could also capitalize on finer spectral characteristics in lichens in general and usnic lichens in particular (Kaasalainen & Rautiainen, 2005; Korpela, 2008; Solheim et al., 2000). For example, usnic acid has a strong yellow reflectance and a strong absorption peak in the UV (Gauslaa, 1984). These unique spectral features of usnic lichens could be utilized for mapping if sensors with narrower bandpasses in the visible wavelengths were used in conjunction with those capable of measuring UV absorption.

Our results support the hypothesis that usnic lichens would be the most detectable lichen cover group. Our model of usnic lichen cover revealed nonlinear relationships with spectral and environmental variables. High usnic lichen cover occurs in lowland boreal forests on alluvial terraces and middle and higher elevation alpine ridges. This spatial pattern is supported by other studies that document high lichen abundance in sandy or rocky soils in lowland forests (Ahti, 1977; Kershaw, 1978) or alpine tundra (Holt et al., 2007).

Our models of non-lichen vegetation groups that are important in caribou diets were also successful with between two and four spectral and environmental predictors. The resulting maps of deciduous and coniferous trees, shrubs and graminoids correspond to known ecological patterns for these vegetation groups. Deciduous trees were most abundant in post-fire areas with warmer or well-drained soils. Conifer abundance peaked in the lower elevations in well-drained, warmer soils inhabited by *P. glauca* or areas underlain by permafrost dominated by *P. mariana*. Areas of high shrub abundance formed a swath in the mid-elevations, dominated by *Betula nana* in colder soils and *A. viride* in wetter, warmer soils. Graminoids were most abundant in flat, mid-elevation, frozen soils encapsulated by the Toklat basin ecoregion subsection.

These maps of continuous vegetation abundance could be used for many types of ecological studies at multiple spatial scales. The maps' utility for improving our understanding of caribou biology must be tested elsewhere but it is plausible that continuous (vs. categorical) measures of the abundance of diet categories will improve our understanding of habitat selection of caribou and other organisms that range over large areas.

Acknowledgments

Thanks to the numerous National Park Service technicians, especially James Walton and Sarah Stehn, who worked over many years to collect the vegetation and environmental data. Thanks also to Layne Adams, Dave Gustine and Kyle Joly for detailed feedback during this project. We are grateful to the three anonymous reviewers who made many useful comments on the draft manuscript. The National Park Service funded this study.

Appendix A. Supplementary data

Supplementary data associated with this article can be found in the online version, at http://dx.doi.org/10.1016/j.rse.2013.05.026. These data include Google maps of the most important areas described in this article.

References

ACIA (2005). *Arctic climate impact assessment.* Cambridge University Press (1042 pp.).
Ahti, T. (1977). Lichens of the boreal coniferous zone. In M. R. D. Seward (Ed.), *Lichen ecology* (pp. 145–181). London: Academic Press.
Bechtel, R., Rivard, B., & Sánchez-Azofeifa, A. (2002). Spectral properties of foliose and crustose lichens based on laboratory experiments. *Remote Sensing of Environment*, *82*, 389–396.
Bonan, G. B., & Shugart, H. H. (1989). Environmental factors and ecological processes in boreal forests. *Annual Review of Ecology and Systematics*, *20*, 1–28.
Chander, G., Markham, B. L., & Helder, D. L. (2009). Summary of current radiometric calibration coefficients for Landsat MSS, TM, ETM+, and EO-1 ALI sensors. *Remote Sensing of Environment*, *113*, 893–903.
Clark, M. H., & Duffy, M. S. (2006). *Soil survey of Denali National Park area, Alaska.* National Cooperative Soil Survey, NRCS and USDA (1617 pp.).
Colby, J. D. (1991). Topographic normalization in rugged terrain. *Photogrammetric Engineering and Remote Sensing*, *57*, 531–537.
Cornelissen, J. H. C., Callaghan, T. V., Alatalo, J. M., & Michelsen, A. (2001). Global change and arctic ecosystems: Is lichen decline a function of increases in vascular plant biomass? *Journal of Ecology*, *89*, 984–994.
Dingman, S. L., & Koutz, F. R. (1974). Relations among vegetation, permafrost, and potential insolation in central Alaska. *Arctic and Alpine Research*, *6*, 37–47.
Franklin, J., Davis, F. W., & Lefebvre, P. (1991). Thematic mapper analysis of tree cover in semiarid woodlands using a model of canopy shadowing. *Remote Sensing of Environment*, *36*, 189–202.
Gauslaa, Y. (1984). Infrared and visible reflectance in different lichen species and its ecological significance. *Holarctic Ecology*, *7*, 13–22.
Gilichinsky, M., Sandström, P., Reese, H., Kivinen, S., Moen, J., & Nilsson, M. (2011). Mapping ground lichens using forest inventory and optical satellite data. *International Journal of Remote Sensing*, *32*, 455–472.
Grime, J. P. (1977). Evidence for the existence of three primary strategies in plants and its relevance to ecological and evolutionary theory. *American Naturalist*, *111*, 1169–1194.
Heggberget, T. M., Gaare, E., & Ball, J. P. (1992). Reindeer (*Rangifer tarandus*) and climate change: Importance of winter forage. *Rangifer*, *22*, 13–31.
Hoge, F. E., & Lyon, P. E. (1996). Satellite retrieval of inherent optical properties by linear matrix inversion of oceanic radiance models: An analysis of model and radiance measurement errors. *Journal of Geophysical Research*, *101*(C7), 16,631–16,648.

Holt, E. A., McCune, B., & Neitlich, P. (2007). Succession and community gradients of arctic macrolichens and their relation to substrate, topography, and rockiness. *Pacific Northwest Fungi*, *2*, 1–21.
Holt, E. A., McCune, B., & Neitlich, P. (2008). Grazing and fire impacts on macrolichen communities of the Seward peninsula, Alaska, U.S.A. *The Bryologist*, *111*, 68–83.
Horler, D. N. H., & Ahern, F. J. (1986). Forestry information content of thematic mapper data. *International Journal of Remote Sensing*, *7*, 405–428.
Jensen, J. R. (2005). *Introductory digital image processing: A remote sensing perspective* (3rd ed.) New Jersey: Pearson Prentice Hall (Chapter 9).
Johnson, C. J., Parker, K. L., & Heard, D. C. (2000). Feeding site selection by woodland caribou in north-central British Columbia. *Rangifer Special*, *12*, 159–172.
Johnson, C. J., Parker, K. L., Heard, D. C., & Seip, D. R. (2004). Movements, foraging habits, and habitat use strategies of northern woodland caribou during winter: Implications for forest practices in British Columbia. *BC Journal of Ecosystems & Management*, *5*, 22–35.
Joly, K., Cole, M. J., & Jandt, R. R. (2007). Diets of overwintering caribou, *Rangifer tarandus*, track decadal changes in Arctic tundra vegetation. *Canadian Field-Naturalist*, *121*, 379–383.
Joly, K., Jandt, R. R., & Klein, D. R. (2009). Decrease of lichens in arctic ecosystems: The role of wildfire, caribou, reindeer, competition and climate in northwestern Alaska. *Polar Research*, *28*, 433–442.
Kaasalainen, S., & Rautiainen, M. (2005). Hot spot reflectance signatures of common boreal lichens. *Journal of Geophysical Research*, *110* (10 pp.).
Kershaw, K. A. (1978). The role of lichens in boreal tundra transition areas. *The Bryologist*, *81*, 294–306.
Korpela, I. S. (2008). Mapping of understory lichens with airborne discrete-return LiDAR data. *Remote Sensing of Environment*, *112*, 3891–3897.
Macander, M. J. (2010). *A surface reflectance calibrated Landsat mosaic (circa 2002) for the Arctic network of national parks.* NPS/ARCN/NRTR — 2010/393. Fort Collins, CO: National Park Service (39 pp.).
Mayor, S. J., Schaefer, J. A., Schneider, D. C., & Mahoney, S. P. (2009). The spatial structure of habitat selection: A caribou's-eye-view. *Acta Oecologica — International Journal of Ecology*, *35*, 253–260.
McCune, B. (2006). Non-parametric habitat models with automatic interactions. *Journal of Vegetation Science*, *17*, 819–830.
McCune, B. (2007). Improved estimates of incident radiation and heat load using non-parametric regression against topographic variables. *Journal of Vegetation Science*, *18*, 751–754.
McCune, B., & Mefford, M. J. (2009). *HyperNiche version 2.13.* Non-parametric multiplicative habitat modeling. Gleneden Beach, Oregon, U.S.A.: MjM Software.
McCune, B., & Mefford, M. J. (2011). *PC-ORD version 6.0. Multivariate analysis of ecological data.* Users guide. Gleneden Beach, Oregon, U.S.A.: MjM Software.
Nordberg, M. L., & Allard, A. (2002). A remote sensing methodology for monitoring lichen cover. *Canadian Journal of Remote Sensing*, *28*, 262–274.
Olthof, I., & Fraser, R. H. (2007). Mapping northern land cover fractions using Landsat ETM+. *Remote Sensing of Environment*, *107*, 496–509.
Petzold, D. E., & Goward, S. N. (1988). Reflectance spectra of subarctic lichens. *Remote Sensing of Environment*, *24*, 481–492.
Rees, W. G., Golubeva, E. I., & Williams, M. (1998). Are vegetation indices useful in the Arctic? *Polar Record*, *34*, 333–336.
Rees, W. G., Tutubalina, O. V., & Golubeva, E. I. (2004). Reflectance spectra of subarctic lichens between 400 and 2400 nm. *Remote Sensing of Environment*, *90*, 281–292.
Riedel, S. M., Epstein, H. E., & Walker, D. A. (2005). Biotic controls over spectral reflectance of Arctic tundra vegetation. *International Journal of Remote Sensing*, *26*, 2391–2405.
Roland, C. A., Oakley, K., Debevec, E. M., & Loomis, T. (2004). *Monitoring vegetation structure and composition at multiple scales in the central Alaska network.* NPS technical report CAKN-001. Fairbanks, Alaska, USA: National Park Service (https://irma.nps.gov/App/Reference/Profile?code¼2190295).
Roland, C. A., Schmidt, J. H., & Nicklen, E. F. (2012). Landscape-scale patterns in tree occupancy and abundance in subarctic Alaska. *Ecological Monographs*, *83*, 19–48.
Russell, D. E., Martell, A. M., & Nixon, W. A. C. (1993). Range ecology of the Porcupine caribou herd in Canada. *Rangifer*, *13*, 1–168.
Schlerf, M., & Atzberger, C. (2006). Inversion of a forest reflectance model to estimate structural canopy variables from hyperspectral remote sensing data. *Remote Sensing of Environment*, *100*, 281–294.
Smith, J., Lin, T., & Ranson, K. (1980). The Lambertian assumption and Landsat data. *Photogrammetric Engineering and Remote Sensing*, *46*, 1183–1189.
Solheim, I., Engelsen, O., Hosgood, B., & Andreoli, G. (2000). Measurement and modeling of the spectral and directional reflection properties of lichen and moss canopies. *Remote Sensing of Environment*, *72*, 78–94.
Stow, D. A., Hope, A. S., & George, T. H. (1993). Reflectance characteristics of Arctic tundra vegetation from airborne radiometry. *International Journal of Remote Sensing*, *14*, 1239.
Stueve, K. M., Isaacs, R. E., Tyrrell, L. E., & Densmore, R. V. (2010). Spatial variability of biotic and abiotic tree establishment constraints across a treeline ecotone in the Alaska range. *Ecology*, *92*, 496–506.
Théau, J., Peddle, D. R., & Duguay, C. R. (2005). Mapping lichen in a caribou habitat of northern Quebec, Canada, using an enhancement classification method and spectral mixture analysis. *Remote Sensing of Environment*, *94*, 232–243.
Viereck, L. A., Dyrness, C. T., Batten, A. R., & Wenzlick, K. J. (1992). *The Alaska vegetation classification. PNW-GTR-286.* Portland, OR: USDA Forest Service Pacific Northwest Research Station (278 pp.).
Viereck, L. A., & Schandelmeier, L. A. (1980). *Effects of fire in Alaska and adjacent Canada: A literature review., Vol. 6*, US Bureau of Land Management, Alaska State Office (124 pp.).
Zhang, J., Rivard, B., & Sánchez-Azofeifa, A. (2005). Spectral unmixing of normalized reflectance data for the deconvolution of lichen and rock mixtures. *Remote Sensing of Environment*, *95*, 57–66.